Article

Multi-objective optimization for maximum fundamental frequency and minimum cost of hybrid graphene/fibre-reinforced nanocomposite laminates

Drosopoulos, Georgios, Gogos, C. and Foutsitzi, G.

Drosopoulos, Georgios orcid iconORCID: 0000-0002-4252-6321, Gogos, C. and Foutsitzi, G. (2023) Multi-objective optimization for maximum fundamental frequency and minimum cost of hybrid graphene/fibre-reinforced nanocomposite laminates. Structures, 54 . pp. 1593-1607.

Structures 54 (2023) 1593–1607

Contents lists available at ScienceDirect

Structures

journal homepage: www.elsevier.com/locate/structures

Multi-objective optimization for maximum fundamental frequency and minimum cost of hybrid graphene/fibre-reinforced nanocomposite laminates

G.A. Drosopoulos [a,b,*], C. Gogos [c], G. Foutsitzi [c]

[a] Discipline of Civil Engineering, University of Central Lancashire, Preston, United Kingdom
[b] Discipline of Civil Engineering, University of KwaZulu-Natal, Durban, South Africa
[c] Department of Informatics and Telecommunications, University of Ioannina, Arta, Greece

ARTICLE INFO

Keywords:
Graphene nanoplatelets (GPLs)
Fundamental frequency
Optimal cost
Laminated nanocomposites
Multi-objective optimization
NSGA II

ABSTRACT

The present article proposes a multi-objective optimization study aiming at the optimal cost-effective design of nano-reinforced laminates. To maximize the fundamental frequency and minimize the cost, a hybrid laminate is studied, introducing both conventional fibres and graphene nanoplatelets reinforcement. A multi-objective genetic algorithm optimization is adopted to provide the optimal natural frequency and cost for the laminate. Optimization is implemented using the Non-dominated Sorting Genetic Algorithm II (NSGA-II), which converges to near-optimal solutions for all scenarios tested. The vibration problem is solved using the finite element method and the first-order shear deformation theory. Effective material properties are derived using micromechanical equations. Different optimization problems are solved using one to four types of design variables, including graphene and fibre distribution along the thickness, layer thickness, and fibre angles. Results indicate that increasing the graphene nanoplatelets content and keeping the minimum fibre content leads to cost-effective design. A drastic increase in the fundamental frequency and decrease in the cost is obtained for the hybrid graphene/fibre-reinforced laminate compared to conventional fibre-reinforced composites.

1. Introduction

Nanocomposite laminates are materials incorporating nano-scale reinforcements, including carbon nanotubes (CNTs) or graphene nanoplatelets (GPLs), to improve mechanical and physical properties. Graphene has been extensively used in several engineering applications in the fields of structural, mechanical and aerospace engineering. Its excellent mechanical properties [1] allow for significant improvement of the mechanical response of composites, even when only a small graphene content is used. This concept of improving the mechanical response of conventional composite materials by introducing advanced nanomaterials with superior properties has been widely investigated in the last few years [2,3].

Various optimization methods are often integrated in numerical studies to provide optimal solutions for significant engineering problems involving vibration, buckling, non-linear static response (damage), optimal weight/cost, or optimal stiffness for composite laminates. Regarding the search method adopted to provide the optimum solution, two main optimization approaches are recognized, namely the gradient-based, deterministic and the gradient-free, stochastic approach. The gradient-based methods may converge fast to the optimal solution, but this will likely be local. The stochastic approaches are appropriate for providing a near-global optimum solution.

Several single-objective optimization studies have been conducted to provide the optimal response of fibre-reinforced composite laminates. In [4], an advanced differential evolution optimization algorithm is adopted to investigate the minimum weight for composite laminate plates. An artificial neural network integrated into a differential evolution optimization scheme is proposed in [5], aiming to investigate the optimal material distribution of bidirectional functionally graded beams under free vibration. In [6] a particle swarm optimization algorithm is adopted to solve a maximum frequency optimization problem for symmetrical laminated composites using the classical laminated plate theory. In [7], a combined genetic algorithm-deep neural network procedure is proposed to optimize laminated cylinders' maximum frequency/gaps to improve accuracy and reduce computational cost. In

* Corresponding author at: Discipline of Civil Engineering, University of Central Lancashire, Preston, United Kingdom.
E-mail address: gdrosopoulos@uclan.ac.uk (G.A. Drosopoulos).

https://doi.org/10.1016/j.istruc.2023.05.118
Received 1 February 2023; Received in revised form 13 May 2023; Accepted 27 May 2023
Available online 9 June 2023

[8], a genetic algorithm is used to optimize the geometry joint parameters of a laminated FRP composite-made bonded tubular gap K-joint based on failure criteria and ply-stacking sequence.

More single-objective optimization problems have been studied within this framework, emphasizing, among others, in the maximum fundamental frequency for composite plates using the Artificial Bee Colony algorithm [9], in the maximum buckling load adopting an improved, different evolution algorithm [10], in optimizing functional graded distributions using a differential evolution algorithm [11] and in minimum weight optimization utilizing standard gradient-based nonlinear programming algorithms [12]. These efforts aim to optimize the mechanical response of composite laminates, using as design variables the fibre angles, the thickness of layers as well as the content of the fibre reinforcement.

An important requirement for industrial applications of composites is the cost-effective design. To achieve this goal, numerical solutions are investigated, minimizing the cost and weight of composite materials. The critical aspect of this effort is to maintain the structural integrity of composites by investigating their response against conventional loading, such as buckling and vibration. Thus, the need for optimal solutions practically arises, which involve more than one objective functions.

In [13], a multi-objective optimization scheme applied to a laminated composite beam is proposed. The objective function is to minimize the weight of the laminate beam and maximize its natural frequency. Design variables are the fibre volume fractions, thickness, and orientation. In [14], a multi-objective optimization method is discussed to achieve high strength and low weight for varying thicknesses. In this case, a fracture criterion (strength) and the mean curvature (weight) are the objective functions, with design variables the fibre orientation and thickness distribution. In [15], a multi-objective design is proposed for laminated composite plates, investigating optimal stiffness properties. The defined objective functions aim to maximize the fundamental frequency and buckling resistance. Pareto-optimal solutions are provided for a range of objective functions, boundary conditions, and load cases. A multi-objective particle swarm optimization scheme is proposed in [16] to solve problems of lightweight design for bi-directional functionally graded beams considering the maximum fundamental frequency and critical buckling load. The material volume fraction in this work is described in both longitudinal and thickness directions. A multi-objective uncertainty optimization approach is proposed in [17] for hybrid composite structures consisting of multiple materials with different types and volume ratios of matrix and fibres. The objective is to maximize natural frequency/gap and minimize cost. An adaptive non-dominated sorting genetic algorithm II (NSGA-II) method is used in this study to optimize the stacking sequence and material patches. In [18] genetic algorithm is used to solve multi-objective optimization problems for hybrid, laminated sandwich panels composed of high-stiffness face sheets and low-stiffness core. Pareto-optimal solutions are derived for several objective functions, including fundamental frequency, frequency gap, buckling load, and cost metrics.

The concept of introducing some nano reinforcement in the form of graphene nanoplatelets or carbon nanotubes has been investigated in the last years in several numerical or experimental studies, aiming to highlight the effectiveness of nano-reinforced laminates [19]. These studies emphasize in the influence of different loading types, focusing, among others, on functionally graded distributions of the nano reinforcement, along the thickness of the laminate [20,21,22]. Investigations can also be found in vibration analysis of graphene-reinforced nanocomposites [23,24,25].

However, while for conventional fibre-reinforced laminates, a significant amount of published work is dedicated to developing single and multi-objective optimization solutions, for these nano-reinforced laminates, fewer optimization studies can be found. In [26], a heuristic optimization technique (genetic algorithm) combined with a gradient-based one is used to investigate the optimal static and dynamic response of bi-directional functionally graded multi-walled carbon nanotube-reinforced composites. In [27], a bees algorithm optimization scheme is adopted to provide the optimal (maximum) natural frequency and the corresponding optimum geometrical and material parameters of a smart sandwich plate, consisting of a porous homogeneous core, two carbon nanotube-reinforced composite layers, and two piezoelectric face sheets. In [28], multi-objective optimization schemes using either particle swarm optimization or the non-dominated sorting genetic algorithm II are adopted to minimize the peak crushing force and maximize the energy absorption for graphene-type multi-cell tubes. In [29], the Bees algorithm determines the optimal natural frequency of imperfect three-dimensional penta-graphene plates.

Recently, the concept of introducing graphene or carbon nanotubes and fibre reinforcement is investigated, leading to three-phase composites. The addition of nano reinforcement, together with fibre reinforcement, is expected to improve the mechanical response and, at the same time, keep the directional properties of fibres. Only limited literature is found on single or multi-objective optimization schemes for three-phase fibre nano-reinforced composites. In [30], stacking sequence optimization of a CNT-fibre-reinforced polymer composite plate is proposed, aiming to maximize the fundamental natural frequency of the structure. Optimization is implemented using a biologically-inspired *meta*-heuristic algorithm called firefly. In [31] Differential Evolution, Nelder Mead and Simulated Annealing optimization algorithms are used to determine the optimal frequency and cost of graphite-flax/epoxy hybrid laminates. Results highlighted the benefits of introducing natural flax fibres in maximizing frequency and minimizing cost for the hybrid laminates. A multi-objective optimization scheme is proposed in [32] for hybrid graphite-glass/epoxy and graphite-flax/epoxy composite plates. The objectives of this problem are to minimize the cost and maximize the frequency gaps. The study proposes that the application of flax fibres can reduce the cost and increase the fundamental frequency, as well as the frequency gaps. In [33], this investigation is extended to multi-objective optimization for buckling load and cost. The simultaneous maximization of fundamental frequency or frequency gap between two consecutive frequencies and cost minimization is studied in [34]. The article considers a hybrid scheme of high-stiffness, graphite-epoxy outer layers, and low-stiffness glass-epoxy core layers. A genetic algorithm scheme is adopted to optimize the discrete variables of the problem. In [35], a Sequential Quadratic Programming optimization scheme is proposed for a three-phase graphene/nanoplatelets fibre-reinforced composite plate, aiming to maximize the fundamental frequency.

This article proposes an optimization study to maximize the fundamental frequency and minimize the cost of a three-phase, graphene nanoplatelets/fibre-reinforced composite plate. To the best of the authors' knowledge, very limited studies are found on multi-objective optimization of three-phase nano-reinforced laminates. In the optimal design of composite laminates, it is crucial to consider fundamental frequency maximization to decrease the risk of resonance caused by external excitations. It should also be noted that cost is another crucial factor for all engineering problems. Therefore, it must be considered in the design and optimization problems of laminated composite materials. Thus, this work aims to cover this gap, highlighting the optimal response of hybrid, three-phase composites, aiming to increase the fundamental frequency and decrease the cost. Emphasis is given on the optimal, cost-effective design of laminates, which use the directional properties of fibres allowing for the non-uniform distribution of graphene nanoplatelets and fibres, along the thickness of the laminate. A finite element analysis code is developed in MATLAB, and a first-order shear deformation theory is used to simulate the vibration response of the laminate. The Non-dominated Sorting Genetic Algorithm II (NSGA-II) is adopted to implement the multi-objective optimization. The study considers a gradually increased number of design variable types from one to four, involving the graphene and fibre content, the layer thickness, and the stacking sequence angles.

2. Finite element model for laminated composite plates

In this section, the first-order shear deformation theory (FSDT) is employed to derive a finite element model for laminated composite plates like the one shown in Fig. 1. A single mechanical displacement field is considered for all layers (equivalent single-layer theory). The plate has length a, width b, total thickness H and consists of N layers with the principal material coordinates of the k-th lamina oriented at an angle θ_k to the laminate coordinate x. The xy − plane coincides with the midplane of the plate, with the z axis being normal to the midplane. The k-th layer is located between the points $z = z_{k-1}$ and $z = z_k$ in the thickness direction.

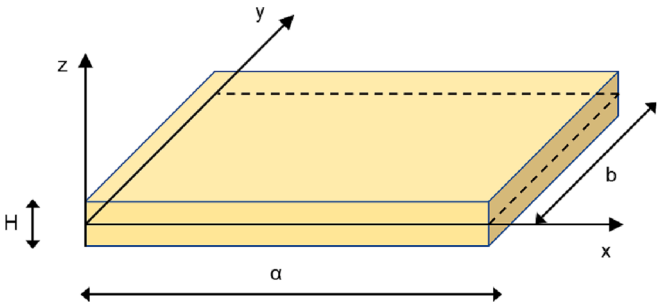

Fig. 1. The composite laminate.

2.1. Mechanical displacement and strains

In this work, the kinematics of the plate are estimated using the first order shear deformation theory (FSDT) which is suitable for moderately thick and thick plates. According to the FSDT, the displacement fields can be written as

$$\boldsymbol{u} = \begin{Bmatrix} u(x,y,z,t) \\ v(x,y,z,t) \\ w(x,y,z,t) \end{Bmatrix} = \begin{Bmatrix} u_0(x,y,t) \\ v_0(x,y,t) \\ w_0(x,y,t) \end{Bmatrix} + z\begin{Bmatrix} \psi_x(x,y,t) \\ \psi_y(x,y,t) \\ 0 \end{Bmatrix} \; or \; \boldsymbol{u} = \boldsymbol{H}\overline{\boldsymbol{u}} \tag{1}$$

where

$$\boldsymbol{H} = \begin{bmatrix} 1 & 0 & 0 & z & 0 \\ 0 & 1 & 0 & 0 & z \\ 0 & 0 & 1 & 0 & 0 \end{bmatrix}, \quad \overline{\boldsymbol{u}} = \left\{u_0, v_0, w_0, \psi_x, \psi_y\right\}^T$$

In Eq. (1), u_0, v_0 and w_0 denote the displacements of a point (x,y) on the mid-plane $(z = 0)$ of the plate and ψ_x, ψ_y are the normal rotations about the y and x-axes, respectively. In addition, a superscript T denotes the transpose of a matrix.

In order to avoid the shear locking effect, the selective integration technique should be implemented. Therefore, the strains at any point of the composite plate are divided in two strain vectors, the in-plane strains $\boldsymbol{\varepsilon}_b$ and the out-of-plane shear strains $\boldsymbol{\varepsilon}_s$ given by

$$\boldsymbol{\varepsilon}_b = \left\{\varepsilon_{xx}, \varepsilon_{yy}, \gamma_{xy}\right\}^T = \boldsymbol{\varepsilon}_{b0} + z\boldsymbol{\kappa},$$

$$\boldsymbol{\varepsilon}_s = \left\{\gamma_{yz}, \gamma_{xz}\right\}^T = \boldsymbol{\varepsilon}_{s0} \tag{2}$$

where

$$\boldsymbol{\varepsilon}_{b0} = \left\{\frac{\partial u_0}{\partial x}, \frac{\partial v_0}{\partial y}, \left(\frac{\partial u_o}{\partial y} + \frac{\partial v_o}{\partial x}\right)\right\}^T,$$

$$\boldsymbol{\kappa} = \left\{\frac{\partial \psi_x}{\partial x}, \frac{\partial \psi_y}{\partial y}, \left(\frac{\partial \psi_x}{\partial y} + \frac{\partial \psi_y}{\partial x}\right)\right\}^T,$$

$$\boldsymbol{\varepsilon}_{s0} = \left\{\frac{\partial w_0}{\partial y} + \psi_y, \frac{\partial w_0}{\partial x} + \psi_x\right\}^T$$

2.2. Constitutive equations

The linear constitutive equations for the k-th orthotropic elastic layer with reference to its principal axes are given by:

$$\begin{Bmatrix} \sigma_1 \\ \sigma_2 \\ \sigma_6 \\ \sigma_4 \\ \sigma_5 \end{Bmatrix}_k = \begin{bmatrix} \overline{Q}_{11} & \overline{Q}_{12} & 0 & 0 & 0 \\ \overline{Q}_{12} & \overline{Q}_{22} & 0 & 0 & 0 \\ 0 & 0 & \overline{Q}_{66} & 0 & 0 \\ 0 & 0 & 0 & \overline{Q}_{44} & 0 \\ 0 & 0 & 0 & 0 & \overline{Q}_{55} \end{bmatrix}_k \begin{Bmatrix} \varepsilon_1 \\ \varepsilon_2 \\ \varepsilon_6 \\ \varepsilon_4 \\ \varepsilon_5 \end{Bmatrix} \tag{3}$$

where σ_i, ε_i are stress and strain components, respectively. $\overline{Q}_{ij}$ are plane-stress reduced stiffness coefficients given by

$$\overline{Q}_{11}^{(k)} = \frac{E_1^{(k)}}{1-\nu_{12}^{(k)}\nu_{21}^{(k)}}, \quad \overline{Q}_{22}^{(k)} = \frac{E_2^{(k)}}{1-\nu_{12}^{(k)}\nu_{21}^{(k)}}, \quad \overline{Q}_{66}^{(k)} = G_{12}^{(k)},$$
$$\overline{Q}_{12}^{(k)} = \frac{\nu_{12}^{(k)}E_2^{(k)}}{1-\nu_{12}^{(k)}\nu_{21}^{(k)}}, \quad \overline{Q}_{44}^{(k)} = k_s G_{23}^{(k)}, \quad \overline{Q}_{55}^{(k)} = k_s G_{13}^{(k)} \tag{4}$$

where $E_1^{(k)}, E_2^{(k)}$ are the longitudinal and transverse moduli, $\nu_{12}^{(k)}, \nu_{21}^{(k)}$ are the Poisson's ratios, $G_{12}^{(k)}, G_{23}^{(k)}, G_{13}^{(k)}$ are the shear moduli of the k^{th} layer and k_s is the shear correction factor taken as $\frac{5}{6}$. For the case of isotropic material, two material constants are required, namely Young's modulus E and Poisson ratio ν. In addition, $Q_{11} = Q_{22}$, $Q_{12} = Q_{11}$ and $Q_{66} = G$ apply with $2G = E/(1+\nu)$.

After transforming Eq. (3) to the global coordinate system (x,y,z) and separating the bending and shear related variables, the constitutive Eq. (3) becomes

$$\boldsymbol{\sigma}_b^{(k)} = \boldsymbol{Q}_b^{(k)}\boldsymbol{\varepsilon}_b, \quad \boldsymbol{\sigma}_s^{(k)} = \boldsymbol{Q}_s^{(k)}\boldsymbol{\varepsilon}_s \tag{5}$$

where $\boldsymbol{\sigma}_b^{(k)} = \left\{\sigma_{xx}, \sigma_{xx}, \tau_{xy}\right\}^T$, $\boldsymbol{\sigma}_s^{(k)} = \left\{\tau_{yz}, \tau_{xz}\right\}^T$ and

$$\boldsymbol{Q}_b^{(k)} = \begin{bmatrix} Q_{11} & Q_{12} & Q_{16} \\ Q_{12} & Q_{22} & Q_{26} \\ Q_{16} & Q_{26} & Q_{33} \end{bmatrix}^{(k)}, \quad \boldsymbol{Q}_s^{(k)} = \begin{bmatrix} Q_{44} & Q_{45} \\ Q_{45} & Q_{55} \end{bmatrix}^{(k)} \tag{6}$$

The detailed expressions for transformed Q_{ij} material constants can be obtained from [36].

2.3. Finite element formulation

In the present study, the finite element method is utilized to obtain the governing equations of motion for the laminated composite plate. The essential idea of finite elements is that a structure may be approximated as an assembly of elements connected at nodes along their boundaries. The laminated composite plate of this study has been discretized using a four-noded isoparametric quadrilateral Lagrangian element with five mechanical degrees of freedom (DOF) per node, namely $u_0, v_0, w_0, \psi_x, \psi_y$.

Using the considerations described above, the generalized displacement field for any nodal point over the plate domain can be expressed as

$$\overline{\boldsymbol{u}}(x,y,t) = \boldsymbol{N}(x,y)\boldsymbol{d}^e(t) = \sum_{j=1}^{4}\left(N_j \boldsymbol{I}_{5x5}\boldsymbol{d}_j^e\right) \tag{7}$$

where $\boldsymbol{d}_j^e = \left\{u_{0j}, v_{0j}, w_{0j}, \psi_{xj}, \psi_{yj}\right\}^T$ corresponds to the j^{th} node of the element and N_j are the Lagrangian shape functions.

Substituting Eq. (7) into Eqs. (2) gives

$$\begin{aligned}\boldsymbol{\varepsilon}_{b0} &= \boldsymbol{B}_b\boldsymbol{d}^e = \sum_{j=1}^{4}\left(\boldsymbol{B}_{bj}\boldsymbol{d}_j^e\right),\\ \boldsymbol{\kappa} &= \boldsymbol{B}_\kappa\boldsymbol{d}^e = \sum_{j=1}^{4}\left(\boldsymbol{B}_{\kappa j}\boldsymbol{d}_j^e\right),\\ \boldsymbol{\varepsilon}_{s0} &= \boldsymbol{B}_s\boldsymbol{d}^e = \sum_{j=1}^{4}\left(\boldsymbol{B}_{sj}\boldsymbol{d}_j^e\right)\end{aligned} \tag{8}$$

where

$$\begin{aligned}\boldsymbol{B}_{bj} &= \begin{bmatrix}\partial_x & 0 & 0 & 0 & 0\\ 0 & \partial_y & 0 & 0 & 0\\ \partial_y & \partial_x & 0 & 0 & 0\end{bmatrix}N_j,\quad \boldsymbol{B}_{\kappa j} = \begin{bmatrix}0 & 0 & 0 & \partial_x & 0\\ 0 & 0 & 0 & 0 & \partial_y\\ 0 & 0 & 0 & \partial_y & \partial_x\end{bmatrix}N_j,\\ \boldsymbol{B}_{sj} &= \begin{bmatrix}0 & 0 & \partial_y & 0 & 1\\ 0 & 0 & \partial_x & 1 & 0\end{bmatrix}N_j\end{aligned} \tag{9}$$

and $\partial_x = \frac{\partial}{\partial x}, \partial_y = \frac{\partial}{\partial y}$.

2.4. Variational principle

The equations of motion for the laminate plate are obtained using the extended Hamilton's principle

$$\delta\int_{t_1}^{t_2}(T-U+W)dt = 0 \tag{10}$$

where t_1 and t_2 are arbitrary time moments, T is the mechanical kinetic energy and U is the mechanical potential energy given by

$$T = \int_\Omega \rho\dot{\boldsymbol{u}}^T\dot{\boldsymbol{u}}d\Omega \tag{11}$$

$$U = \frac{1}{2}\int_\Omega \boldsymbol{\varepsilon}_b^T\boldsymbol{\sigma}_b d\Omega + \frac{1}{2}\int_\Omega \boldsymbol{\varepsilon}_s^T\boldsymbol{\sigma}_s d\Omega \tag{12}$$

In the above equations, ρ, Ω are the mass density and the volume of the whole plate structure and a dot represents partial derivative with respect to time t.

Finally, the virtual work δW done by the external forces is defined by the following equation

$$\delta W = \delta\boldsymbol{u}^T\boldsymbol{f}_c + \int_{A_1}\delta\boldsymbol{u}^T\boldsymbol{f}_S dA + \int_\Omega \delta\boldsymbol{u}^T\boldsymbol{f}_V d\Omega \tag{13}$$

where $\boldsymbol{f}_c$ denotes the concentrated forces and $\boldsymbol{f}_S, \boldsymbol{f}_V$ denote the surface and volume forces, respectively. Also, A_1 is the surface area where the surface forces are applied.

Using the displacements relations (1) and the discretization of mechanical displacements (7), the element kinetic energy can be discretized as

$$T^e = \frac{1}{2}\int_\Omega \rho\dot{\bar{\boldsymbol{u}}}^T\boldsymbol{H}^T\boldsymbol{H}\dot{\bar{\boldsymbol{u}}}d\Omega = \frac{1}{2}\dot{\boldsymbol{d}}^{eT}\left(\int_\Omega \rho\boldsymbol{N}^T\boldsymbol{H}^T\boldsymbol{H}\boldsymbol{N}d\Omega\right)\dot{\boldsymbol{d}}^e = \frac{1}{2}\dot{\boldsymbol{d}}^{eT}\boldsymbol{M}^e\dot{\boldsymbol{d}}^e \tag{14}$$

Since the whole structure consists of N layers, the element mass matrix $\boldsymbol{M}^e$ can be written as

$$\boldsymbol{M}^e = \sum_{k=1}^{N}\int_{\Omega_k}\rho^{(k)}\boldsymbol{N}^T\boldsymbol{H}^T\boldsymbol{H}\boldsymbol{N}d\Omega_k = \int_{A_e}\boldsymbol{N}^T\begin{bmatrix}I_0 & 0 & 0 & I_1 & 0\\ 0 & I_0 & 0 & 0 & I_1\\ 0 & 0 & I_0 & 0 & 0\\ I_1 & 0 & 0 & I_2 & 0\\ 0 & I_1 & 0 & 0 & I_2\end{bmatrix}\boldsymbol{N}dA \tag{15}$$

where

$$I_i = \sum_{k=1}^{N}\int_{z_k}^{z_{k+1}}\rho^{(k)}z^i dz,\qquad i = 0,1,2 \tag{16}$$

and A_e is the in-plane area of the element.

Using the constitutive relations, the mechanical strain energy U can be written as

$$\begin{aligned}U^e = \frac{1}{2}\sum_{k=1}^{N}\int_{\Omega_k}&\left(\boldsymbol{\varepsilon}_{b0}^T\boldsymbol{Q}_b^{(k)}\boldsymbol{\varepsilon}_{b0} + \boldsymbol{\varepsilon}_{b0}^T z\boldsymbol{Q}_b^{(k)}\boldsymbol{\kappa} + \boldsymbol{\kappa}^T z\boldsymbol{Q}_b^{(k)}\boldsymbol{\varepsilon}_{b0} + \boldsymbol{\kappa}^T z^2\boldsymbol{Q}_b^{(k)}\boldsymbol{\kappa}\right)d\Omega_k\\ &+ \frac{1}{2}\sum_{k=1}^{N}\int_{\Omega_k}\boldsymbol{\varepsilon}_s^T\boldsymbol{Q}_s^{(k)}\boldsymbol{\varepsilon}_s d\Omega_k\end{aligned} \tag{17}$$

Substituting the relations (8), (9) in the above relation, U can be written as

$$\begin{aligned}U^e &= \frac{1}{2}\boldsymbol{d}^{eT}\left(\int_{A_e}\left(\boldsymbol{B}_b^T\boldsymbol{A}\boldsymbol{B}_\kappa + \boldsymbol{B}_b^T\boldsymbol{B}\boldsymbol{B}_\kappa + \boldsymbol{B}_\kappa^T\boldsymbol{B}\boldsymbol{B}_b + \boldsymbol{B}_\kappa^T\boldsymbol{D}\boldsymbol{B}_\kappa\right)dA\right.\\ &\quad\left.+\int_{A_e}\left(\boldsymbol{B}_s^T\boldsymbol{E}\boldsymbol{B}_s\right)dA\right)\boldsymbol{d}^e\\ &= \frac{1}{2}\mathbf{d}^{eT}\boldsymbol{K}^e\mathbf{d}^e\end{aligned} \tag{18}$$

where the element stiffness matrix can be written as

$$\boldsymbol{K}^e = \int_{A_e}\begin{bmatrix}\boldsymbol{B}_b\\ \boldsymbol{B}_\kappa\end{bmatrix}^T\begin{bmatrix}\boldsymbol{A} & \boldsymbol{B}\\ \boldsymbol{B} & \boldsymbol{D}\end{bmatrix}\begin{bmatrix}\boldsymbol{B}_b\\ \boldsymbol{B}_\kappa\end{bmatrix}dA + \int_{A_e}\left(\boldsymbol{B}_s^T\boldsymbol{E}\boldsymbol{B}_s\right)dA \tag{19}$$

The material matrices involved in the above relation are given as

$$\begin{aligned}(\boldsymbol{A},\boldsymbol{B},\boldsymbol{D}) &= \sum_{k=1}^{N}\int_{z_k}^{z_{k+1}}\boldsymbol{Q}_b^{(k)}(1,z,z^2)dz,\\ \boldsymbol{E} &= \sum_{k=1}^{N}\int_{z_k}^{z_{k+1}}\boldsymbol{Q}_s^{(k)}dz\end{aligned} \tag{20}$$

It should be noted that for the last term of stiffness matrix of Eq. (19) associated with the transverse shear strains, a selective integration rule should be employed in order to avoid the shear locking effect.

The virtual work done by the mechanical forces is given by

$$\delta W = \delta\boldsymbol{d}^{eT}\boldsymbol{N}^T\boldsymbol{f}_c + \delta\boldsymbol{d}^{eT}\int_{A_1}\boldsymbol{N}^T\boldsymbol{f}_S dA + \delta\boldsymbol{d}^{eT}\int_\Omega \boldsymbol{N}^T\boldsymbol{H}^T\boldsymbol{f}_V d\Omega = \delta\boldsymbol{d}^{eT}\boldsymbol{F}_m^e \tag{21}$$

2.5. Governing equations

By substituting the energy terms (14), (18) and (21) into Hamilton's principle Eq. (10) and by assembling the element equations, the overall equation of motion of the structure is obtained as

$$\boldsymbol{M}\ddot{\boldsymbol{d}} + \boldsymbol{K}\boldsymbol{d} = \boldsymbol{F}_m \tag{22}$$

where $\boldsymbol{d}$ is the global vector of mechanical coordinates, $\boldsymbol{M}$, $\boldsymbol{K}$ are the global mass and stiffness matrices and $\boldsymbol{F}_m$ is the global vector of mechanical forces.

2.6. Free vibration analysis

Free vibration can be treated as a subset problem in Eq. (22). Indeed, dropping the force terms and assuming harmonic solution of the form $\boldsymbol{u} = \boldsymbol{u}_o e^{i\omega t}$, the above equation result in the following generalized eigenvalue problem

$$\left(\boldsymbol{K} - \omega^2\boldsymbol{M}\right)\boldsymbol{u}_o = \boldsymbol{0} \tag{23}$$

where $\omega, \boldsymbol{u}_o$ are the eigenfrequencies and eigenvectors, respectively. The natural frequencies can be found from the nontrivial solution of Eq. (23). A MATLAB code has been developed to implement the presented finite element model. A reduced integration technique is adopted to avoid shear and membrane locking during computation. This method is previously developed by the authors to solve single-objective problems for three-phase graphene/fibre reinforced laminated nanocomposite plates [35]. The solution to the eigenvalue problem (23) is also implemented within MATLAB using the function "eig". This function uses Cholesky factorization of the mass matrix $\boldsymbol{M}$ to compute the generalized

eigenvalues since the stiffness matrix $\boldsymbol{K}$ is symmetric and the mass matrix $\boldsymbol{M}$ is symmetric positive-definite.

3. Effective material properties for the three-phase laminate

The optimal response of a three-phase, graphene and fibre reinforced polymer nanocomposite is investigated in this work. According to the main concept of the study, low content of graphene nanoplatelets is added to the conventional fibre-reinforced laminate to improve the vibration response and reduce the cost, contributing to the cost-effective design.

In order to derive the effective material properties of the three-phase laminate, a two-phase graphene-reinforced matrix is initially considered. The graphene-reinforced matrix is then reinforced by fibre reinforcement. The effective material properties of the graphene-reinforced matrix are obtained using the Halpin-Tsai model and the rule of mixture. The same micromechanical homogenization approach is also used in the published literature to derive the effective material properties of graphene-reinforced laminates [37,38,39].

A second set of micromechanics equations is utilized to determine the effective material properties of the overall, three-phase graphene-fibre reinforced laminate [4,35].

3.1. Graphene-reinforced matrix

The material properties, namely Young's modulus, Shear modulus, Poisson's ratio, and density, are calculated for the graphene-reinforced matrix using micromechanical equations [37,38,39]. Subscripts GPL, M, and GM denote graphene nanoplatelets (GPL), the matrix (M), and the graphene-reinforced matrix (GM). The effective Young's modulus for the graphene-reinforced matrix is provided by

$$E_{GM} = \left(\frac{3}{8}\frac{1+\xi_L\eta_L V_{GPL}}{1-\eta_L V_{GPL}} + \frac{5}{8}\frac{1+\xi_w\eta_w V_{GPL}}{1-\eta_w V_{GPL}}\right)E_M \tag{24}$$

where V_{GPL} is the volume content of GPLs. The parameters ξ_L and ξ_w are given in Eq. (25) in terms of the length (l_{GPL}), the width (w_{GPL}) and the thickness (h_{GPL}) of GPLs

$$\xi_L = 2\frac{l_{GPL}}{h_{GPL}}, \qquad \xi_w = 2\frac{w_{GPL}}{h_{GPL}} \tag{25}$$

The symbols η_L and η_w in Eq. (24) are calculated in terms of Young's moduli E_{GPL} of the graphene nanoplatelets and E_M of the matrix as

$$\eta_L = \frac{(E_{GPL}/E_M)-1}{(E_{GPL}/E_M)+\xi_L}, \qquad \eta_w = \frac{(E_{GPL}/E_M)-1}{(E_{GPL}/E_M)+\xi_w} \tag{26}$$

The volume content of graphene nanoplatelets is computed in terms of its weight fraction W_{GPL} as

$$V_{GPL} = \frac{W_{GPL}}{W_{GPL}+(\rho_{GPL}/\rho_M)(1-W_{GPL})} \tag{27}$$

where ρ_{GPL} and ρ_M represent the mass densities of graphene nanoplatelets and the polymer matrix, respectively. Poisson's ratio, Shear modulus and the density of the graphene-reinforced matrix are given by

$$v_{GM} = v_{GPL}V_{GPL} + v_M(1-V_{GPL}) \tag{28}$$

$$G_{GM} = \frac{E_{GM}}{2(1+v_{GM})} \tag{29}$$

$$\rho_{GM} = \rho_{GPL}V_{GPL} + \rho_M(1-V_{GPL}) \tag{30}$$

3.2. Graphene and fibre reinforced matrix

The three-phase material is obtained by considering unidirectional and continuous fibre reinforcement applied to the graphene-reinforced matrix. The effective material properties for the three-phase graphene-fibre reinforced laminate are determined using the following micromechanical relations [4,35]

$$E_{11} = E_{F11}V_F + E_{GM}(1-V_F) \tag{31}$$

$$E_{22} = E_{GM}\left(\frac{E_{F22}+E_{GM}+(E_{F22}-E_{GM})V_F}{E_{F22}+E_{GM}-(E_{F22}-E_{GM})V_F}\right) \tag{32}$$

$$G_{12} = G_{13} = G_{GM}\left(\frac{G_{F12}+G_{GM}+(G_{F12}-G_{GM})V_F}{G_{F12}+G_{GM}-(G_{F12}-G_{GM})V_F}\right) \tag{33}$$

$$G_{23} = \frac{E_{22}}{2(1+v_{23})} \tag{34}$$

$$v_{12} = v_{F12}V_F + v_{GM}(1-V_F) \tag{35}$$

$$v_{23} = v_{F12}V_F + v_{GM}(1-V_F)\left(\frac{1+v_{GM}+v_{12}E_{GM}/E_{11}}{1-v_{GM}^2+v_{12}v_{GM}E_{GM}/E_{11}}\right) \tag{36}$$

$$\rho = \rho_F V_F + \rho_{GM}(1-V_F) \tag{37}$$

In the above equations, the subscripts GM and F refer to graphene-reinforced matrix and fibres, respectively. The fibre volume content is represented by V_F and the density of fibres by ρ_F.

4. Formulation of multi-objective optimization problems

4.1. Uniform layer thickness

In this section, the proposed multi-objective optimization approach aiming at the optimal vibration response and cost-effective design of a graphene-fibre reinforced composite laminate is initially formulated for the case of uniform layer thickness. Objectives of this formulation are to maximize the fundamental frequency and minimize the cost of the laminate, utilizing one or two types of design variables, namely, the graphene nanoplatelets and the fibre content. Constraints are also applied to the optimization, providing an upper limit to the overall contents of graphene nanoplatelets and fibres and limits to graphene and fibre volume contents, per layer.

In the following formulations, the fibre and the graphene volume contents are denoted by V_{Fi} and V_{GPLi}, for every layer i. For the laminate plate of N layers shown in Fig. 1, with dimensions $a \times b$, uniform layer thickness h and overall thickness H, the constraint for the upper limit of the overall fibre volume content of the laminate is provided by the following inequality

$$abh\sum_{i=1}^{N} V_{Fi} \leqslant abHV_{F\max} \Rightarrow \frac{h}{H}\sum_{i=1}^{N} V_{Fi} \leqslant V_{F\max} \tag{38}$$

where $V_{F\max}$ is the maximum fibre volume content of the laminate. When uniform layer thickness is adopted, $Nh = H$, indicating that relation (38) becomes

$$\begin{aligned} &\frac{h}{Nh}\sum_{i=1}^{N} V_{Fi} \leqslant V_{F\max} \Rightarrow \frac{1}{N}\sum_{i=1}^{N} V_{Fi} \leqslant V_{F\max} \\ &\Rightarrow (N=8), \quad \frac{1}{8}\sum_{i=1}^{8} V_{Fi} \leqslant V_{F\max} \end{aligned} \tag{39}$$

As shown in (39), 8 layers are considered in this study (N = 8). A similar constraint is formulated for the overall graphene nanoplatelets content:

$$\frac{1}{8}\sum_{i=1}^{8} V_{GPLi} \leq V_{GPLmax} \tag{40}$$

noticing that V_{GPLmax} represents the maximum graphene content for the laminate.

The multi-objective optimization problem can now be formulated for the case of uniform layer thickness as follows:

$$\begin{aligned} &\max \ f(V_{Fi}, V_{GPLi}) = \omega \ \ (Fundamental\ Frequency) \\ &\quad \min C_L(V_{Fi}, V_{GPLi}) = c \ \ (Cost) \end{aligned} \tag{41a}$$

subject to

$$\frac{1}{8}\sum_{i=1}^{8} V_{Fi} \le V_{Fmax} \tag{41b}$$

$$\frac{1}{8}\sum_{i=1}^{8} V_{GPLi} \le V_{GPLmax} \tag{41c}$$

$$V_{GPLi} \ge 0 \tag{41d}$$

$$0.10 \le V_{Fi} \le 0.60 \tag{41e}$$

According to inequalities (41d) and (41e), some limits for graphene nanoplatelets and fibre contents are considered for each layer. The fundamental frequency for the laminate is determined using the first-order shear deformation theory and the finite element method, as provided in section 2. The cost of the laminate C_L is also defined in equation (42), as the sum of the cost of fibres C_F, graphene nanoplatelets C_{GPL} and matrix C_M

$$\begin{aligned} C_L(V_{Fi},\ V_{GPLi}) &= \sum_{i=1}^{8}(C_{Fi} + C_{GPLi} + C_{Mi}) \\ &= abh\sum_{i=1}^{8}[\rho_F\, V_{Fi}c_F + \rho_{GPL}\, V_{GPLi}c_{GPL} + \rho_M\,(1 - V_{Fi} - V_{GPLi})c_M\,] \end{aligned} \tag{42}$$

In relation (42) the cost per unit mass for fibres, graphene nanoplatelets and matrix, is denoted, respectively, by c_F, c_{GPL} and c_M. An expression for the non-dimensional cost is eventually used in the calculations, defined as the ratio of the cost given in (42) over the cost of a reference isotropic plate, of dimensions $a \times b$, thickness equal to the total thickness of the three-phase laminate ($= Nh$), density ρ_0 and cost per unit mass equal to 1:

$$\begin{aligned} c &= \frac{C_L(V_{Fi},\ V_{GPLi})}{abNh\rho_0} \\ &= \frac{abh\sum_{i=1}^{8}[\rho_F\, V_{Fi}c_F + \rho_{GPL}\, V_{GPLi}c_{GPL} + \rho_M\,(1 - V_{Fi} - V_{GPLi})c_M\,]}{abNh\rho_0} \\ &= \frac{\sum_{i=1}^{8}[\rho_F\, V_{Fi}c_F + \rho_{GPL}\, V_{GPLi}c_{GPL} + \rho_M\,(1 - V_{Fi} - V_{GPLi})c_M\,]}{N\rho_0} \end{aligned} \tag{43}$$

4.2. Non-uniform layer thickness

For a laminate with non-uniform layer thicknesses, each layer may have a different thickness, indicating that the layer thickness h_i now becomes a design variable. Optimization problems with 3 and 4 types of design variables, namely graphene nanoplatelets and fibre contents, layer thickness and fibre angle, are then formulated.

For this case, the constraints for the total fibre volume content and for the total graphene nanoplatelets content, are provided below

$$\begin{aligned} ab\sum_{i=1}^{N} h_i V_{Fi} \le abHV_{Fmax} &\Rightarrow \frac{1}{H}\sum_{i=1}^{N} h_i V_{Fi} \le V_{Fmax} \\ &\Rightarrow (N = 8),\ \frac{1}{H}\sum_{i=1}^{8} h_i V_{Fi} \le V_{Fmax} \end{aligned} \tag{44}$$

$$\frac{1}{H}\sum_{i=1}^{8} h_i V_{GPLi} \le V_{GPLmax} \tag{45}$$

The corresponding optimal design problem is formulated as follows:

$$\begin{aligned} \max f\left(V_{Fi}, V_{GPLi}, \frac{h_i}{H}, \theta_i\right) &= \omega \quad (Fundamental\ Frequency) \\ \min C_L\left(V_{Fi}, V_{GPLi}, \frac{h_i}{H}, \theta_i\right) &= c \quad (Cost) \end{aligned} \tag{46a}$$

subject to

$$\frac{1}{H}\sum_{i=1}^{8} h_i V_{Fi} \le V_{Fmax} \tag{46b}$$

$$\frac{1}{H}\sum_{i=1}^{8} h_i V_{GPLi} \le V_{GPLmax} \tag{46c}$$

$$V_{GPLi} \ge 0 \tag{46d}$$

$$0.10 \le V_{Fi} \le 0.60 \tag{46e}$$

$$-90^o \le \text{Fibre angles } \theta_i \le 90^o \tag{46f}$$

$$\sum_{i=1}^{N} \frac{h_i}{H} \le 1 \tag{46g}$$

Similar to the case of uniform layer thickness, the cost of the laminate C_L is defined as the sum of the cost of fibres C_F, graphene nanoplatelets C_{GPL} and matrix C_M

$$\begin{aligned} C_L\left(V_{Fi}, V_{GPLi}, \frac{h_i}{H}, \theta i\right) &= \sum_{i=1}^{8}(C_{Fi} + C_{GPLi} + C_{Mi}) \\ = ab\left(\sum_{i=1}^{8}[h_i\rho_F\, V_{Fi}c_F] + \sum_{i=1}^{8}[h_i\rho_{GPL}V_{GPLi}c_{GPL}]\ + \sum_{i=1}^{8}[h_i\rho_{\mathrm{M}}(1 - V_{Fi} - V_{GPLi})c_M]\right) \end{aligned} \tag{47}$$

The expression for the non-dimensional cost is defined for the case of non-uniform thickness, as the ratio of cost of the three-phase laminate, over the cost of a reference isotropic plate, of dimensions $a \times b$, thickness equal to the total thickness of the three-phase laminate ($= H$), density ρ_0 and cost per unit mass equal to 1:

$$\begin{aligned} c &= \frac{C_L\left(V_{Fi}, V_{GPLi}, \frac{h_i}{H}, \theta i\right)}{abH\rho_0} \\ &= \frac{ab\left(\sum_{i=1}^{8}[h_i\rho_F V_{Fi}c_F] + \sum_{i=1}^{8}[h_i\rho_{GPL}V_{GPLi}c_{GPL}] + \sum_{i=1}^{8}[h_i\rho_M(1-V_{Fi}-V_{GPLi})c_M]\right)}{abH\rho_0} \\ &= \frac{\sum_{i=1}^{8}[h_i\rho_F V_{Fi}c_F] + \sum_{i=1}^{8}[h_i\rho_{GPL}V_{GPLi}c_{GPL}] + \sum_{i=1}^{8}[h_i\rho_M(1-V_{Fi}-V_{GPLi})c_M]}{H\rho_0} \end{aligned} \quad (48)$$

5. NSGA II

NSGA-II [40], which stands for Non-dominated Sorting Genetic Algorithm version II is a famous algorithm with a record of good performance in solving several multi-objective optimization problems. NSGA-II is a modified genetic algorithm based on the concept of dominance. Dominance is defined for solutions x_1 and x_2 as follows. Solution x_1 dominates solution x_2 if either x_1 is no worse than x_2 in all objectives or x_1 is strictly better than x_2 in at least one objective. All non-dominated solutions form a set of solutions known as the Pareto set (or Pareto Front). NSGA-II tries to find solutions as close as possible to the optimal Pareto Front and simultaneously as diverse as possible. This is achieved by performing non-dominated sorting of solutions while exploiting the crowding distance metric, which is the Manhattan Distance of solutions in the n-dimensional objective space. In each generation, new candidate solutions are generated by combining existing solutions. Iteratively, non-dominated solutions are kept for the next generation and removed from the current generation until the size of the new generation is reached, or no more new solutions can be generated. Each batch of non-dominated solutions is sorted according to the crowding distance, giving infinity values to extreme points to be kept for the next generation. NSGA-II, as its name suggests, is the successor of the simpler algorithm NSGA, which lacks the concepts of crowding and has a less efficient procedure for computing the sorted list of non-dominated solutions. The success of NSGA-II led to many variations of the algorithm, including R-NSGA-II, U-NSGA-II, and NSGA-III [41]. It should be noted that many other multi-objective optimization algorithms exist that can be used instead of NSGA-II, such as MOEA/D (Multi-Objective Evolutionary Algorithm with Decomposition), SPEA2 (Strength Pareto Evolutionary Algorithm 2), and others. MOEA/D is a family of algorithms that decomposes the problem into simpler single or multi-objective subproblems, which are then optimized concurrently and cooperatively. SPEA2 uses an elitism approach that assigns fitness to solutions based on the strength values of the solutions that dominate them and breaks fitness ties based on density information. The wealth of multi-objective optimization algorithms becomes apparent through software packages like PlatEMO [42], which in its 4.0 release, supports more than 200 evolutionary algorithms. Most of these algorithms aim at multi-objective problems.

Table 1
Comparison of non-dimensional frequency $\Omega = \omega a^2\sqrt{\rho_m/(E_m H^2)}$ derived from this study with published research, for the case of laminated [0/90/0/90/0] CNT-reinforced plates, with simply supported (SSSS) boundary conditions and thickness/length ratio 0.1 ($H/a = 0.1$)

Pattern	Method	Mode			
		1	2	3	4
Uniformly distributed CNT with volume fraction $V_{CNT} = 0.11$	Present/ Mesh 5x5	14.6364	19.7484	19.7484	30.2317
	Present/ Mesh 10x10	14.3104	19.5075	19.5075	28.0341
	Present/ Mesh 12x12	14.2772	19.4830	19.4830	27.8178
	Ref. [43]	14.2952	19.4565	19.4589	27.1005
	Ref. [44]	14.2773	19.4141	19.4191	27.0981
Uniformly distributed CNT with volume fraction $V_{CNT} = 0.14$	Present/ Mesh 5x5	15.7050	20.1010	20.1010	31.9455
	Present/ Mesh 10x10	15.3773	19.8557	19.8557	29.7699
	Present/ Mesh 12x12	15.3438	19.8308	19.8308	29.5539
	Ref. [43]	15.2954	19.7801	19.7842	28.6689
	Ref. [44]	15.2702	19.7613	19.7666	28.6659
Uniformly distributed CNT with volume fraction $V_{CNT} = 0.17$	Present/ Mesh 5x5	18.1351	24.7090	24.7090	37.5627
	Present/ Mesh 10x10	17.7265	24.4075	24.4075	34.8013
	Present/ Mesh 12x12	17.6850	24.3769	24.3769	34.5299
	Ref. [43]	17.7233	24.3158	24.3201	33.6782
	Ref. [44]	17.7087	24.2906	24.2908	33.6735

6. Verification of the proposed approach

6.1. Verification of the vibration analysis

To validate the finite element model which is used for the vibration analysis, the natural frequencies of a CNT-reinforced laminated plate

Table 2
Material properties of GPLs, matrix, and glass fibres.

Material	E_{11}(GPa)	E_{22} (GPa)	G_{12} (GPa)	ν_{12}	Density (kg/m^3)
GPL	1010	1010	$E_{11}/(2(1+\nu))$	0.186	1060
Matrix	3	3	$E_{11}/(2(1+\nu))$	0.34	1200
Glass fibres	72.4	72.4	$E_{11}/(2(1+\nu))$	0.20	2400

with SSSS boundary conditions are calculated and compared with the results reported in [43,44]. Geometric properties of the plate are $a = b = 1m$ and thickness $H = 0.1m$. The lay-up stacking sequence of the plate is [0/90/0/90/0]. For the CNT-reinforced plate, the material properties of the matrix are given as $E_m = 2.5\,\text{GPa}$, $\nu_m = 0.34$ and $\rho_m = 1150\,Kg/m^3$ at room temperature 300 ^oK. Material properties of single-walled CNTs (SWCNTs) are given as $E_{11}^{CNT} = 5.6466\,\text{TPa}$, $E_{22}^{CNT} = 7.08\,\text{TPa}$, $G_{12}^{CNT} = 1.9455\,\text{TPa}$, $G_{13}^{CNT} = G_{23}^{CNT} = G_{12}^{CNT}$, $\nu_{12}^{CNT} = 0.175$ and $\rho^{CNT} = 1400\,Kg/m^3$. For the different volume fractions of CNTs that are tested, parameters η_i are $\eta_1 = 0.149, \eta_2 = 0.934, \eta_3 = \eta_2$ for $V_{CNT} = 0.11$, $\eta_1 = 0.15$, $\eta_2 = 0.941, \eta_3 = \eta_2$ for $V_{CNT} = 0.14$ and $\eta_1 = 0.149, \eta_2 = 1.381, \eta_3 = \eta_2$ for $V_{CNT} = 0.17$. Table 1 shows the comparison of the first four non-dimensional frequencies ($\Omega = \omega a^2\sqrt{\rho_m/(E_m H^2)}$) of (uniformly distributed) CNT-reinforced plates for different V_{CNT} values. As shown in Table 1, frequencies obtained from the finite element model used in this article are close to the ones provided in published literature.

6.2. Verification of the optimization approach

To verify the optimization approach which is presented in this article, comparisons of the results obtained from the proposed formulation and results presented in literature are conducted. The material properties which are used in this and subsequent sections, are given in Table 2. Furthermore, the following values are adopted for graphene nanoplatelets dimensions: $l_{GPL} = 2.5\,\mu\text{m}$, $w_{GPL} = 1.5\,\mu\text{m}$, $h_{GPL} = 1.5\,\text{nm}$.

For the results which are presented in this section, as well as the results which are discussed in the following sections of the article, the fundamental frequency ω is provided in the form of the non-dimensional frequency Ω:

$$\Omega = \omega H\sqrt{\frac{\rho_M}{E_M}} \tag{49}$$

where E_M and ρ_M denote the Young's modulus and mass density of the polymer matrix and H is the total thickness of the laminate. It is noted that the number of the design variables which are considered for each problem solved in the article, indicates the number of design variable types. Each design variable is assigned a different value over the layers, by the solution of the optimization problem.

An initial comparison of the natural frequencies obtained by the proposed method and those found in published literature is presented in [35] for both an isotropic plate and a two-phase, graphene nanoplatelets-reinforced laminate with uniform GPLs content and layer thickness. As discussed in [35], this comparison between the proposed method and published results is satisfactory.

Furthermore, to verify the natural frequencies derived from the proposed method for the case of a three-phase graphene nanoplatelet/fibre-reinforced laminate, a comparison is conducted in [35] between the natural frequencies derived from the present work and the ones determined using commercial finite element software (ABAQUS). Several models have been considered for this comparison, including laminates with different layer numbers, stacking sequences, and boundary conditions. For the implementation in the commercial software, 4-node shell elements have been used. Results presented in [35] indicate a satisfactory agreement between the proposed method and the commercial software.

Table 3
Comparison of maximum fundamental frequencies Ω obtained from the proposed multi-objective optimization approach and from reference [35] for an 8-layered, GPLs/glass fibre-reinforced square laminate with V_{GPL} content as the design variable, subject to GPLs weight fractions $W_{GPLi} \geq 0$ and $W_{GPLmax} = 1.25\%$, thickness/length ratio 0.1, and SSSS boundary conditions.

Stacking sequence	Fibre contents	Method	Optimal V_{GPL} per layer	Ω
$[0/90/0/90]_{\text{anti-s}}$	Glass 30%	Ref. [35]	$[0.0540/0.0025/0/0]_s$	0.1766
		Present	$[0.0545/0.0020/0/0]_s$	0.1766

Table 4
Comparison of maximum fundamental frequencies Ω obtained from the proposed multi-objective optimization approach and from reference [35] for an 8-layered, GPLs/glass fibre-reinforced square laminate with GPLs and fibre volume content as the design variables, subject to GPLs weight fractions $W_{GPLi} \geq 0$ and $W_{GPLmax} = 1.25\%$, fibre volume contents $0.1 \leq V_{Fi} \leq 0.6$, $V_{Fmax} = 30\%$, thickness/length ratio 0.1, and SSSS boundary conditions.

Stacking sequence	Method	Optimal V_{GPL} per layer	Optimal V_F per layer	Ω
$[0/90/0/90]_{\text{anti-s}}$	Ref. [35]	$[0.0394/0.0169/0/0]_s$	$[0.6/0.4/0.1/0.1]_s$	0.1864
	Present	$[0.0383/0.0182/0/0]_s$	$[0.6/0.17/0.1/0.1]_s$	0.1848

To further validate the multi-objective optimization approach of the present study, a comparison with the results provided in [35] is conducted for a three-phase GPLs/glass fibre-reinforced composite laminate. Since in [35] a maximum frequency single-objective optimization scheme is proposed, the comparison is conducted using the maximum (optimal) frequency derived from the multi-objective approach of the current work. It is noted that in [35] a Sequential Quadratic Programming algorithm (SQP) is used to implement the single-objective optimization scheme. An alternative multi-objective optimization approach is adopted in the present study, which uses the NSGA-II (Non-dominated Sorting Genetic Algorithm version II), relying on the concept of dominance.

Results are compared for the case of one and two design variables, namely, the GPLs and glass fibre content. It is noted that the results which are shown in [35], provide the distribution of graphene nanoplatelets as weight fraction for every layer. In Tables 3 and 4, these values have been converted to GPLs volume content, using equation (27).

As shown in Tables 3 and 4, this comparison results in a good agreement between the maximum (optimal) natural frequencies obtained by the proposed multi-objective optimization approach and the ones provided in [35], for the problems with one and two design variables. It is observed that the distributions of the GPLs and fibre reinforcements along the thickness of the laminate, as obtained by the two approaches, are also similar.

7. Results and discussion

Results derived from the proposed multi-objective optimization study, aiming to maximize the fundamental frequency and minimize the cost of an 8-layered, three-phase, graphene nanoplatelets/fibre-reinforced composite laminate, are discussed in this section. In the developed models, uniform layer thickness, using one and two design variables (GPLs and fibre volume content), and non-uniform layer thickness, using three and four design variables (GPLs and fibre volume content, thickness ratio and fibre angle) are considered. It is noted that all the design variables which are used in this study are continuous.

For the results presented in the following sections for the problems with one, two, and three design variables, namely GPLs content, fibre content, and thickness ratio, an antisymmetric angle-ply ($[0/90/0/90]_{\text{anti-s}}$) stacking sequence has been adopted for the laminate. In addition, a square plate is considered, with an aspect ratio $a/b = 1$ and simply supported boundary conditions (SSSS). The total thickness over the edge length ratio H/a is chosen as equal to 0.1. The thickness ratio h/H, which is one of the design variables for the case of non-uniform layer thickness, is defined as the ratio of the thickness of each layer over the overall thickness of the laminate. For all simulations, the following limits are assigned: GPLs weight fractions $W_{GPLi} \geq 0$ and

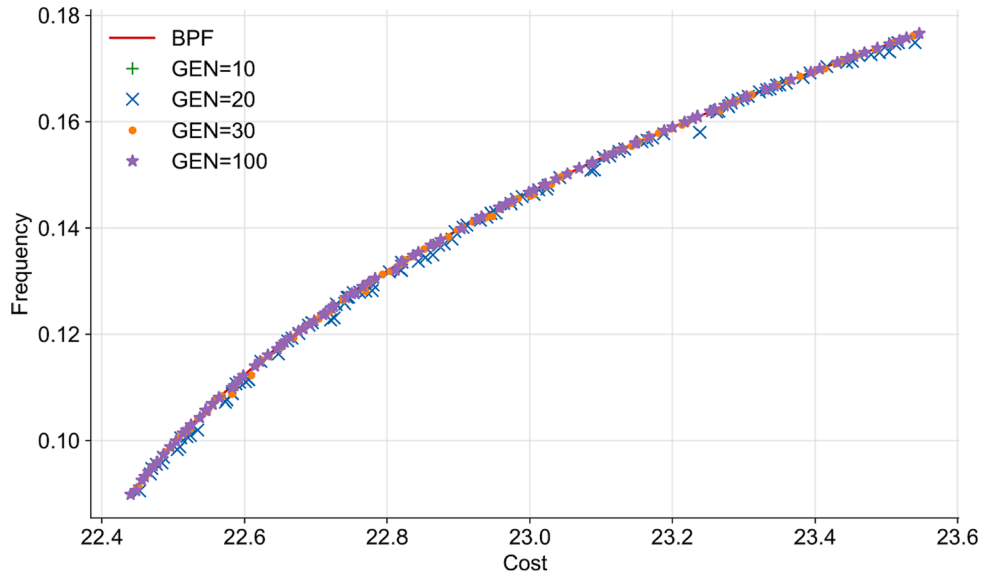

Fig. 2. Multi-objective optimization using GPLs content as single design variable and 30% uniform fibre content.

Table 5
Selected pareto optimal solutions yielding low, medium and high objective values for the multi-objective optimization problem with GPL content as design variable.

Fibre contents	Pareto optimal V_{GPL} per layer	Total V_{GPL}	Ω (non-dimensional frequency)	c (non-dimensional cost)
Glass 30%	$[0/0.004/0/0]_s$	0.008	0.0905	22.45
	$[0.0078/0/0/0]_s$	0.0156	0.1115	22.59
	$[0.017/0.002/0/0]_s$	0.038	0.1320	22.81
	$[0.021/0/0.0005/0]_s$	0.043	0.1370	22.87
	$[0.0545/0.002/0/0]_s$	0.113	0.1766	23.55

W_{GPLmax} = 1.25%, fibre volume contents $0.1 \leq V_{Fi} \leq 0.6$ and V_{Fmax} = 30%.

To derive the results, which are provided in the following sections, a set of numerical experiments were executed on a workstation equipped with an Intel Core i7 7700 K @4.2 GHz CPU and 32 GB DDR4 RAM. The implementation of the NSGA-II algorithm provided by the PlatEMO software [42], which operates over MATLAB 2018b, was adopted. Ten runs were performed for each experiment. Each run took about 5000 s and used a set of 100 individuals that evolved for 100 generations. The solutions of the last generation of each run were used for calculating the Base Pareto Front (BPF), which served as a substitution for the unknown Optimal Pareto Front (OPF).

7.1. Optimal results for the case of uniform layer thickness

Results from the models with one and two design variables, namely the GPLs and fibre content, obtained for uniform layer thickness, are discussed in this section. Fig. 2 shows the evolution of the Pareto of a

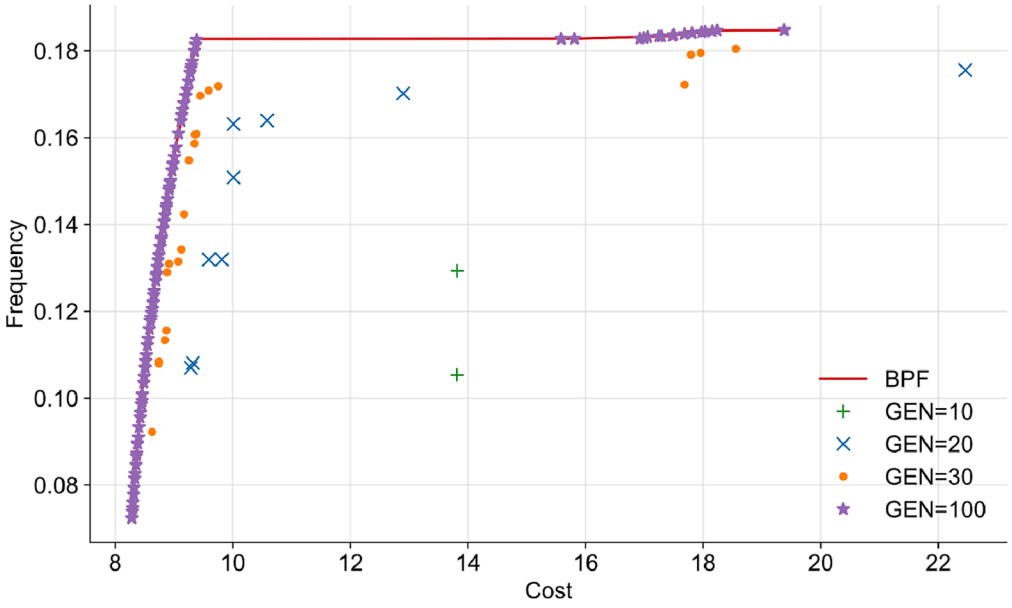

Fig. 3. Multi-objective optimization using two design variables, namely, GPLs and fibre contents.

Table 6
Selected pareto optimal solutions yielding low, medium and high objective values for the multi-objective optimization problem with GPL and fibre contents as design variables.

Pareto optimal V_{GPL} per layer	Pareto optimal V_F per layer	Total V_{GPL}	Total V_F	Ω (non-dimensional frequency)	c (non-dimensional cost)
$[0/0/0/0]_s$	$[0.1/0.1/0.1/0.1]_s$	0	0.8	0.0724	8.28
$[0.00514/0/0/0]_s$	$[0.1/0.1/0.1/0.1]_s$	0.0103	0.8	0.0909	8.40
$[0.01524/0/0/0]_s$	$[0.1/0.1/0.1/0.1]_s$	0.0305	0.8	0.1116	8.58
$[0.023/0/0/0]_s$	$[0.1/0.1/0.1/0.1]_s$	0.0460	0.8	0.1320	8.73
$[0.026/0/0/0]_s$	$[0.1/0.1/0.1/0.1]_s$	0.0520	0.8	0.1370	8.79
$[0.0517/0/0/0]_s$	$[0.1/0.1/0.1/0.1]_s$	0.1034	0.8	0.1766	9.29
$[0.0558/0.0006/0.0001/0]_s$	$[0.46/0.1/0.1/0.1]_s$	0.1130	1.52	0.1828	15.81
$[0.0383/0.01817/0/0]_s$	$[0.6/0.17/0.1/0.1]_s$	0.1129	1.94	0.1848	19.38

single run alongside the BPF for the multi-objective optimization problem with one design variable, the GPLs content. It can be seen that the solutions of even early generations (10, 20, 30) almost coincide with the BPF. This also occurs for the rest of the runs, suggesting that the approach can identify high-quality Pareto optimal solutions.

In Table 5, some Pareto optimal solutions of the 100th generation of the same run are depicted. Optimal solutions that correspond to extreme frequency values and some solutions for intermediate frequencies are shown in this table. For each frequency, different values of the design variables are obtained from optimization, noticing that more GPL reinforcement is needed to accommodate higher frequencies. The results provided in this and subsequent sections, represent a set of solutions that are non-dominated with respect to both objectives (i.e., frequency and cost). This means that it is not possible to find another solution that improves one objective without worsening the other. So, a human decision maker should be responsible for determining the relative importance of each objective, and identify solutions that should be judged as most suitable.

According to these results, a pattern of solutions is recognized, which is also expected for the subsequent optimization problems. Thus, as higher optimal frequencies are derived from multi-objective optimization, an increasing optimal cost arises due to the increase of the GPLs reinforcement (design variable). This increase in the GPLs content is attributed to the demand for higher frequencies, enabling the optimization algorithm to increase the nano-reinforcement content to accommodate this demand. On the contrary, when low optimal cost values are approximated, the frequencies which are obtained from optimization are significantly reduced, leading to a lower content of nano-reinforcement.

Therefore, for the lowest frequency and cost values of Table 5, a limited content of nano-reinforcement arises. As the frequency increases, the GPLs content also increases, with more GPLs reinforcement assigned to the outer layers of the laminate. Since the outer layers contribute more than the middle layers to the laminate's stiffness, the vibration response is improved in this case.

For the case that two design variables are defined in multi-objective optimization, namely the graphene and fibre contents, a new Pareto solution is derived, as shown in Fig. 3. It is observed that for an increasing number of generations (20, 30, 100), solutions approach the BPF. The sharp turn on the top left corner shown in Fig. 3 (and in some of the subsequent Pareto diagrams) denotes that at the higher end of frequency values, very small increases have the adverse effect of sending the cost values to a much higher range.

To further investigate the provided results, the optimal design variables and values of the objective functions are given in Table 6 for the case of low, middle, and high frequencies. It is observed that for the lowest frequency (and cost), no graphene reinforcement is assigned, and only the minimum content of fibre reinforcement per layer is used. As optimal frequencies gradually increase, non-zero GPLs content is obtained, with more reinforcement assigned to the outer layers.

Table 7
Selected pareto optimal solutions yielding low, medium and high objective values for the multi-objective optimization problem of a two-phase fibre-reinforced laminate with fibre content as design variable.

Pareto optimal V_F per layer	Total V_F	Ω (non-dimensional frequency)	c (non-dimensional cost)
$[0.1/0.1/0.1/0.1]_s$	0.8	0.0724	8.29
$[0.46/0.1/0.1/0.1]_s$	1.52	0.0907	14.76
$[0.6/0.4/0.1/0.1]_s$	2.4	0.1079	22.44

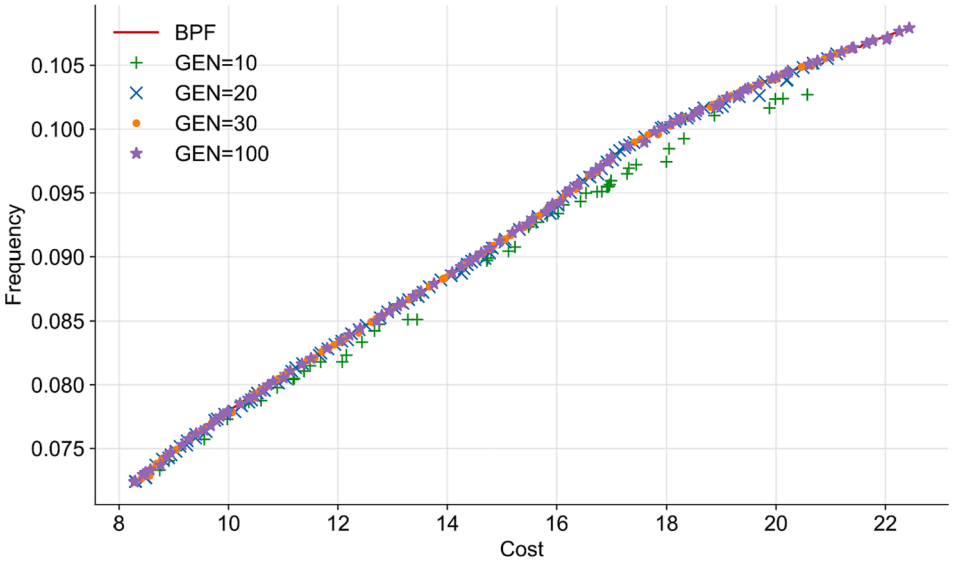

Fig. 4. Multi-objective optimization for a two-phase fibre-reinforced laminate, using one design variable, namely, the fibre volume content.

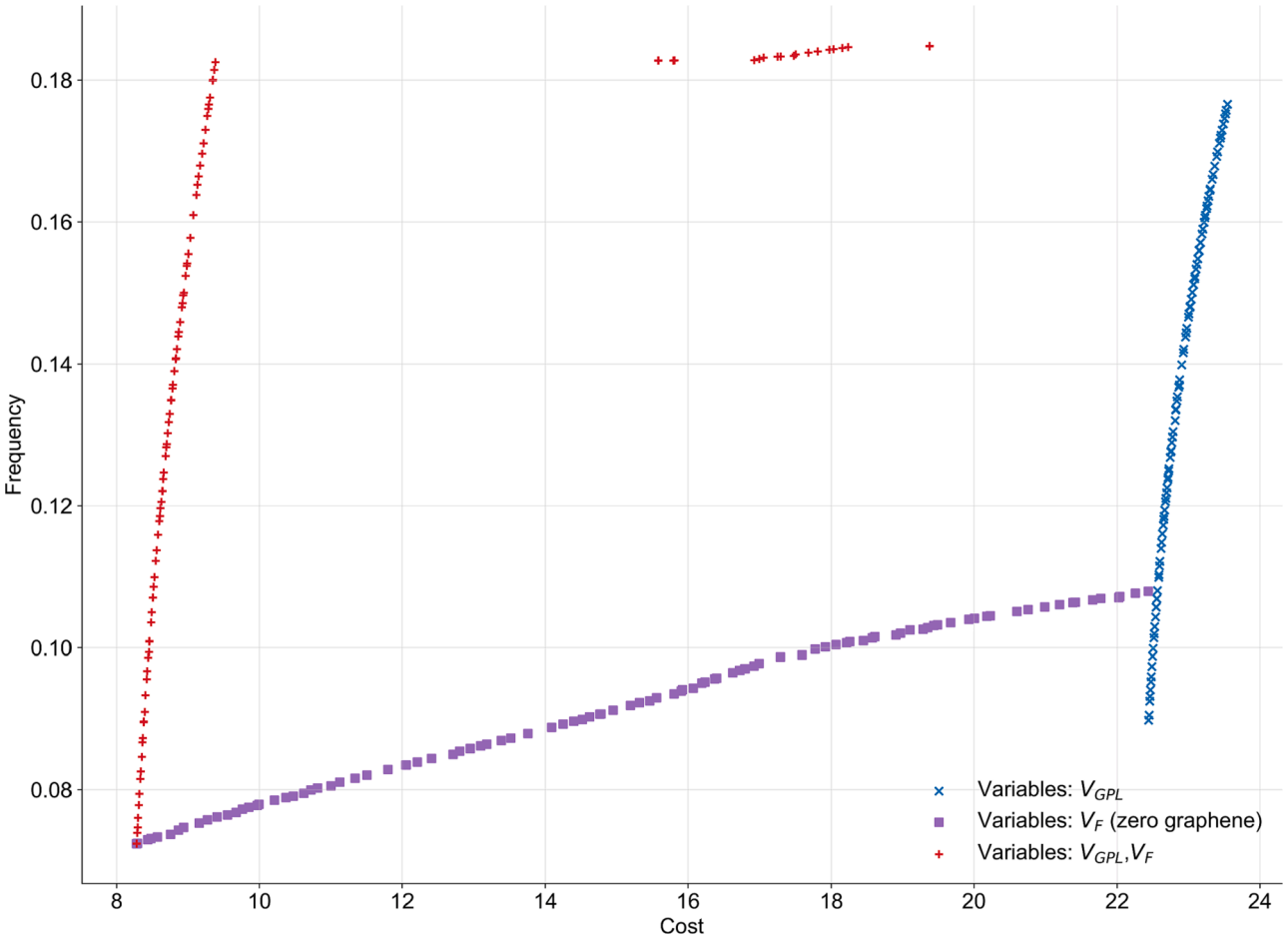

Fig. 5. Multi-objective optimization for the three-phase laminates with one (GPLs content) and two design variables (GPLs and fibre contents) and for the two-phase fibre-reinforced laminate with one design variable (fibre content).

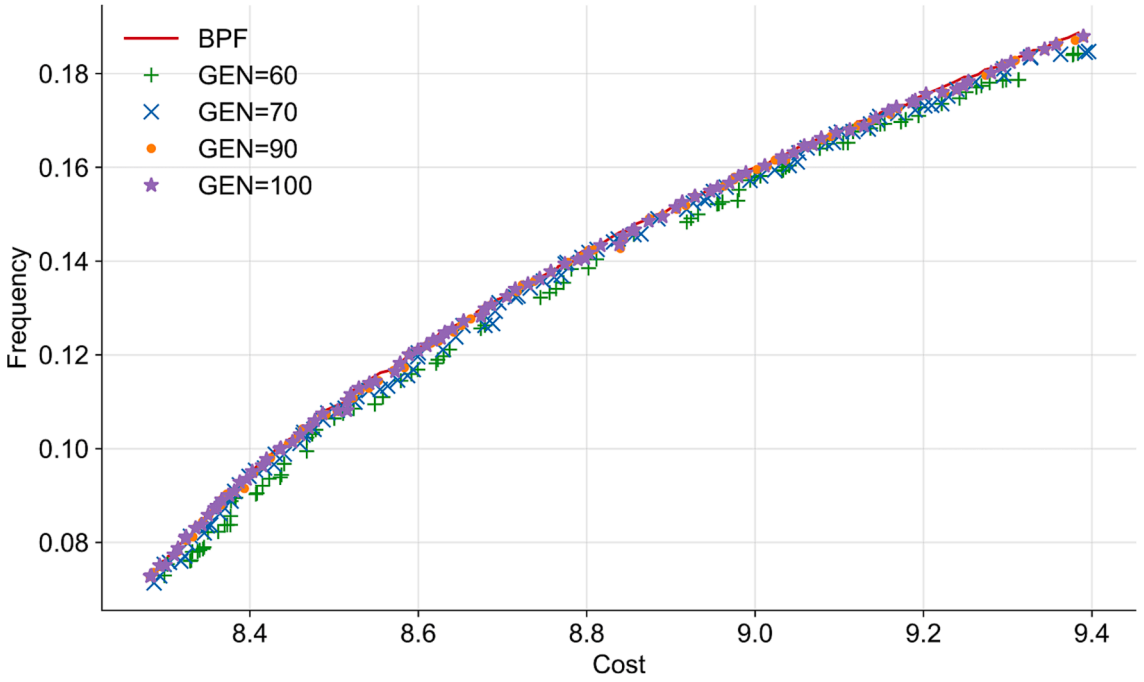

Fig. 6. Multi-objective optimization using three design variables, namely, GPLs content, fibre content and thickness ratio.

Comparison between Table 5 (GPLs content as single design variable, uniform fibre distribution equal to 30%) and Table 6 (GPLs and fibre contents as design variables) can then be conducted to highlight the beneficial influence of the three-phase material, which is studied in this article. To allow for this comparison, approximately equal optimal frequencies are provided in Tables 5 and 6.

In particular, for the same optimal frequencies derived from the problem with one design variable (Table 5), a significantly reduced non-dimensional optimal cost arises when two design variables are considered (Table 6). This is observed for all frequencies of Table 5, which correspond to frequencies from row 2 to row 6 of Table 6. The optimal cost is almost three times lower than the cost obtained at the same frequencies when only one design variable is used.

As observed in Table 6, the solution of the optimization problem provides the minimum content of fibre reinforcement (10% per layer) and gradually increases the graphene content as optimal frequencies increase. The excellent mechanical properties of graphene increase the optimal fundamental frequency even for a low overall GPLs content. For the highest optimal frequencies (the last two frequencies of Table 6), the fibre volume content is also gradually increased. This is accompanied by a significant increase of the optimal cost.

To highlight the contribution of GPLs reinforcement on the optimal vibration response, results of the proposed optimization study are presented next, for the case of a two-phase, fibre-reinforced laminate with no graphene reinforcement. Fig. 4 indicates a good convergence to the optimal Pareto front for an increased number of generations.

In Table 7, optimal results derived for the two-phase laminate are provided in frequency values similar to the ones recorded from the optimization of the three-phase laminate with non-uniform GPLs and fibre content (Table 6). According to the second row of Table 7, the optimal cost is higher by 75.7% than the one obtained for the GPLs/fibre-reinforced laminate (Table 6), at approximately the same maximum frequency. In addition, the maximum optimal frequency that can be achieved for the two-phase laminate (last row of Table 7) is 41.6% lower than the one derived for the three-phase laminate (Table 6). This maximum frequency of the two-phase laminate is obtained at a cost 15.8% higher than that obtained at the maximum frequency of the three-phase laminate (Table 6).

To provide a holistic representation of the optimal solutions for the cases of one and two design variables, the corresponding Pareto solutions derived from 100 generations are given in the diagrams of Fig. 5. It is clearly shown that the diagram representing the solutions from the problem with two design variables (GPLs and fibre contents) is located upper and left in the cartesian coordinate system, compared to the diagram derived from the problem with one design variable (GPLs content). Thus, considering two reinforcing materials (GPLs and fibres) drastically improves the optimal response since lower optimal costs and higher optimal frequencies are derived in this case.

The comparison of the results obtained from the three-phase laminate with two design variables (GPLs and fibre contents) and the two-phase fibre-reinforced laminate with one design variable (fibre content) is also shown in Fig. 5. It is observed that at the same optimal costs, optimal frequencies are significantly higher for the three-phase laminate, highlighting the contribution of GPLs reinforcement to the optimal vibration response.

7.2. Optimal results for the case of non-uniform layer thickness

When non-uniform layer thickness is considered, the thickness ratio is a new design variable. Optimization problems with three and four design variables, namely, the GPLs and fibre contents, the thickness ratio and the fibre angles, are then formulated.

For the problem with three design variables (GPLs content, fibre content, thickness ratio), simulations converge to the BPF for an increased number of generations, as shown in Fig. 6. To further investigate the results of this multi-objective optimization study, the design variables and the corresponding optimal frequency and cost functions are provided in Table 8. Frequency values close to the ones presented in Tables 5 and 6 are given in Table 8, to allow for a comparison of the optimization output. It is observed that as the maximum frequency gradually increases in Table 8, the GPLs content of the outer layers also increases. On the contrary, the fibre volume content remains constant and equal to the minimum content, for all simulations shown in Table 8.

By comparing the first 6 rows of Tables 6 (two design variables and uniform thickness) and 8 (three design variables and non-uniform layer thickness), it is noted that for approximately the same maximum frequency values, Table 8 provides only marginally reduced optimal costs, comparing to costs shown in Table 6. However, a significant difference in the optimal costs arises for the seventh and eighth rows of Tables 6 and 8, which correspond to the highest maximum frequency values.

In particular, for the case of two design variables (Table 6) the optimal costs shown in the seventh and eighth rows increase more than 50% and 100%, respectively, compared to the cost given in the sixth row on the same table. It is also observed that this sharp increase in the optimal cost is accompanied by increased fibre volume content in these rows of Table 6. This means that since the maximum graphene content has been reached in the seventh and eighth row of Table 6, the optimization algorithm attempts to increase also the fibre volume content. Although the cost of fibres is significantly lower than the cost of graphene, the overall cost still increases sharply since significant quantities of fibre volume content are involved.

On the contrary, for the problem with non-uniform thickness and three design variables, the optimal cost does not significantly increase for the seventh and eighth rows of Table 8. Thus, for the highest optimal frequencies, the solution with three design variables manages to keep the cost significantly lower, about 50% and 100%, than the one obtained at the same frequency values from the problem with two design variables (Table 6). It is also observed that there is no increase in the fibre volume content in this case (Table 8). This highlights the beneficial influence of using non-uniform layer thickness within optimization with more design variables.

Next, four design variables are introduced, the GPLs and fibre

Table 8
Selected pareto optimal solutions yielding low, medium and high objective values for the multi-objective optimization problem with GPLs content, fibre content and thickness ratio as design variables.

Pareto optimal V_{GPL} per layer	Pareto optimal V_F per layer	Pareto optimal thickness ratio h/H	Total V_{GPL}	Total V_F	Ω (non-dimensional frequency)	c (non-dimensional cost)
$[0/0/0/0]_s$	$[0.1/0.1/0.1/0.1]_s$	$[0.05/0.15/0.15/0.15]_s$	0	0.8	0.0728	8.28
$[0.007/0/0/0]_s$	$[0.1/0.1/0.1/0.1]_s$	$[0.06/0.15/0.15/0.15]_s$	0.014	0.8	0.0909	8.38
$[0.029/0/0/0]_s$	$[0.1/0.1/0.1/0.1]_s$	$[0.05/0.15/0.15/0.15]_s$	0.058	0.8	0.1116	8.52
$[0.052/0.001/0/0]_s$	$[0.1/0.1/0.1/0.1]_s$	$[0.05/0.15/0.15/0.15]_s$	0.106	0.8	0.1325	8.71
$[0.052/0/0/0]_s$	$[0.1/0.1/0.1/0.1]_s$	$[0.06/0.15/0.14/0.15]_s$	0.104	0.8	0.1378	8.76
$[0.1/0.00014/0.00058/0.00021]_s$	$[0.1/0.1/0.1/0.1]_s$	$[0.06/0.15/0.15/0.14]_s$	0.202	0.8	0.1766	9.24
$[0.124/0/0/0]_s$	$[0.1/0.1/0.1/0.1]_s$	$[0.05/0.15/0.15/0.15]_s$	0.248	0.8	0.1840	9.32
$[0.121/0/0/0.000143]_s$	$[0.1/0.1/0.1/0.1]_s$	$[0.06/0.15/0.14/0.15]_s$	0.242	0.8	0.1879	9.39

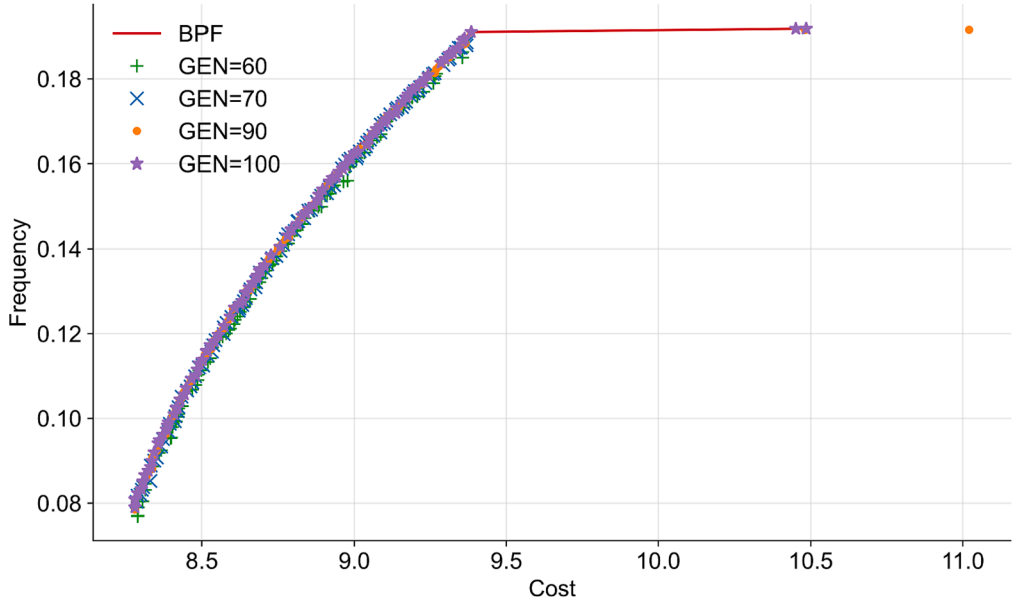

Fig. 7. Multi-objective optimization using four design variables, namely, GPLs content, fibre content, thickness ratio and fibre angle.

Table 9
Selected pareto optimal solutions yielding low, medium and high objective values for the multi-objective optimization problem with GPLs content, fibre content, thickness ratio and fibre angles as design variables.

Pareto optimal V_{GPL} per layer	Pareto optimal V_F per layer	Pareto optimal thickness ratio h/H	Pareto optimal stacking sequence	Total V_{GPL}	Total V_F	Ω (non-dimensional frequency)	c (non-dimensional cost)
$[0/0/0/0]_s$	$[0.1/0.1/0.1/0.1]_s$	$[0.05/0.14/0.15/0.15]_s$	$[42/46/-39/-41]_s$	0	0.8	0.0790	8.28
$[0.0067/0/0/0]_s$	$[0.1/0.1/0.1/0.1]_s$	$[0.06/0.14/0.15/0.15]_s$	$[50/41/-45/-56]_s$	0.0134	0.8	0.0920	8.34
$[0.022/0/0/0]s$	$[0.1/0.1/0.1/0.1]_s$	$[0.06/0.14/0.15/0.15]_s$	$[48/-38/-40/-54]_s$	0.044	0.8	0.1116	8.49
$[0.043/0/0.0001/0]_s$	$[0.1/0.1/0.1/0.1]_s$	$[0.06/0.15/0.15/0.15]_s$	$[59/38/-38/-35]_s$	0.0862	0.8	0.1333	8.68
$[0.053/0/0/0]_s$	$[0.1/0.1/0.1/0.1]_s$	$[0.05/0.15/0.15/0.15]_s$	$[31/47/-52/-45]_s$	0.106	0.8	0.1385	8.73
$[0.109/0/0.0001/0]_s$	$[0.1/0.1/0.1/0.1]_s$	$[0.05/0.15/0.15/0.15]_s$	$[28/46/-44/-25]_s$	0.2182	0.8	0.1775	9.19
$[0.108/0/0.0003/0]_s$	$[0.1/0.1/0.1/0.1]_s$	$[0.06/0.14/0.15/0.15]_s$	$[27/47/-45/-29]_s$	0.2166	0.8	0.1847	9.30
$[0.129/0/0/0]_s$	$[0.1/0.1/0.1/0.1]_s$	$[0.05/0.15/0.15/0.15]_s$	$[42/47/-38/-45]_s$	0.258	0.8	0.1890	9.36
$[0.133/0.0001/0/0]_s$	$[0.1/0.15/0.1/0.1]_s$	$[0.05/0.15/0.15/0.15]_s$	$[42/47/-40/-31]_s$	0.2662	0.9	0.1919	10.48

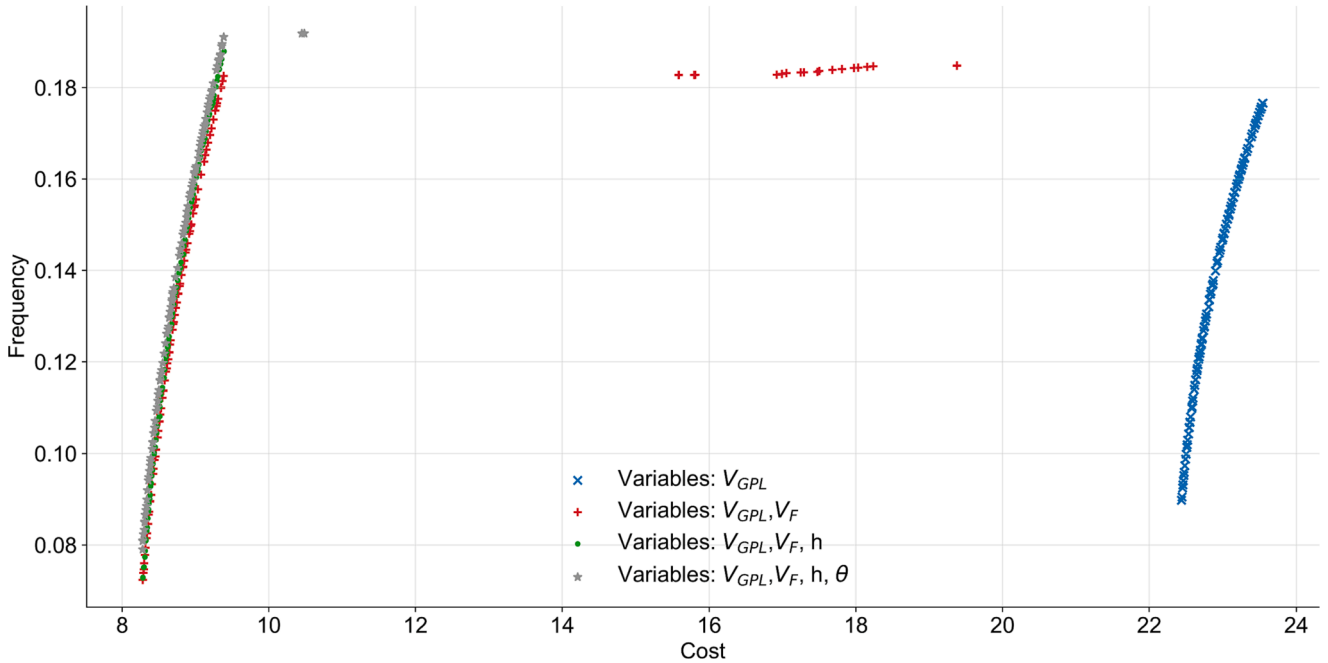

Fig. 8. Multi-objective optimization for the cases of one, two, three and four design variables.

content, the thickness ratio, and the fibre angles. Fig. 7 indicates a good convergence of the optimization simulations to the BPF. Similar to the previous discussions, the optimal frequency and cost values, and the optimal design variables, are given in Table 9. To compare with previous results, the optimal frequencies in Table 9 are similar to the ones provided in the simulations with one, two, and three design variables.

For the first eight rows of Table 9, slightly lower optimal costs are obtained compared to the costs derived from the case of three design variables shown in Table 8. In the last row of Table 9, a higher optimal frequency is achieved, reaching a 2.1% increase, compared to the maximum possible frequency that can be derived for the case of three design variables and shown in the last row of Table 8. According to Table 9, the fibre contents start increasing in this case, leading to a significant increase almost equal to 12% of the optimal cost, compared to the previous row of Table 9 with minimum fibre content.

A similar trend is observed in the case of two design variables (Table 6), thus, denoting increase of the fibre content accompanied by a sharp increase of the optimal cost at maximum frequency levels. However, the maximum optimal frequency achieved in the last row of Table 9 is 3.8% higher than the corresponding of Table 6, obtained at 45.9% lower optimal cost. In all cases, optimization results indicate that increasing the content of GPLs reinforcement is more effective in keeping the cost low than increasing the content of fibre reinforcement. This highlights the beneficial influence of graphene nanoplatelets on cost-effective design.

To summarize the solutions which are derived from the multi-objective optimization problems with one to four design variables, diagrams of the Pareto solutions (100 generations) are provided in Fig. 8. It is indicated that for the highest optimal frequencies, the solution of the problem with non-uniform thickness and three design variables is achieved at significantly lower cost compared to the solution of the problem with uniform layer thickness and two design variables. According to Fig. 8, slightly lower costs at the same frequencies arise for the case of four design variable, compared to the case of three design variables. In addition, a small increase of the highest frequency is achieved for the problem with four design variables, accompanied by a significant increase in the optimal cost.

Fig. 8 also highlights the gradual improvement of the optimal solutions as the number of the design variables increases. It is clear that the problem with the GPLs content as the single design variable, uniform fibre content and layer thickness, results in the solution with the highest optimal costs, compared to the cases of non-uniform fibre reinforcement and layer thickness. Significantly improved response in terms of optimal costs-frequencies is also obtained from the problem with four design variables, with respect to the one with two design variables (non-uniform GPLs and fibre contents).

8. Conclusions

A multi-objective optimization study is presented in this article for a hybrid graphene/fibre-reinforced composite laminate. The work aims to predict the optimal solution that maximizes the frequency and minimizes the cost of the laminate. Optimization is implemented using the Non-dominated Sorting Genetic Algorithm II (NSGA-II). To simulate the vibration response of the laminate, first-order shear deformation theory is adopted in a finite element model developed in MATLAB. Cost-effective optimal design is achieved by solving four optimization problems introducing one to four types of design variables, namely, the graphene nanoplatelets and fibre content, the layer thickness, and the fibre orientation. The goal of the research is to quantify the improvement of the vibration response and the cost reduction, for the increasing number of design variables.

When no graphene reinforcement is considered, the maximum optimal frequency of the conventional two-phase fibre-reinforced laminate is 41.6% lower than the one derived for the three-phase graphene/fibre-reinforced laminate, with non-uniform graphene and fibre volume contents. The optimal cost, which is obtained at the maximum frequency for the two-phase composite, is higher by 15.8% than the one of the graphene/fibre-reinforced laminate. Therefore, a small content of graphene reinforcement drastically increases frequencies and reduces the cost compared to conventional fibre-reinforced laminates.

All results showed that that increasing the graphene volume content and keeping the minimum fibre volume content lead to the most cost-effective design. When the limit for the maximum graphene content is reached, and the optimization solution increases the fibre volume content to achieve higher optimal frequencies, a sharp increase in the cost is obtained. In addition, by increasing the number of design variables from one (graphene nanoplatelets content) to two (graphene and fibre contents), three (graphene, fibre contents, layer thickness) and four (graphene, fibre contents, layer thickness, and fibre angles), optimal frequencies gradually increase, and costs decrease. The highest optimal frequency is obtained from the problem with four design variables, resulting in an increase equal to 2.1% compared to the maximum optimal frequency derived from the model with three design variables.

This research can be extended by introducing more objective functions, like maximum buckling load, providing a more holistic representation of the optimal response. Extensions to optimal functionally graded distributions are also left for future investigation.

Declaration of Competing Interest

The authors declare that they have no known competing financial interests or personal relationships that could have appeared to influence the work reported in this paper.

Acknowledgments

The first co-author was supported by the Greek Diaspora Fellowship Program, Stavros Niarchos Foundation, co-organized by Fulbright Foundation.

References

[1] Zhao S, Zhao Z, Yang Z, Ke LiaoLiang, Kitipornchai S, Yang J. Functionally graded graphene reinforced composite structures: A review. Eng Struct 2020;210:110339.
[2] Reddy B, editor. Advances in Diverse Industrial Applications of Nanocomposites. Rijeka, Croatia: Intech; 2011.
[3] Ebrahimi F, editor. Nanocomposites - New Trends and Developments. Rijeka, Croatia: Intech; 2012.
[4] Vo-Duy T, Ho-Huu V, Do-Thi TD, Dang-Trung H, Nguyen-Thoi T. A global numerical approach for lightweight design optimization of laminated composite plates subjected to frequency constraints. Compos Struct 2017;159:646–55.
[5] Truong TT, Lee S, Lee J. An artificial neural network-differential evolution approach for optimization of bidirectional functionally graded beams. Compos Struct 2020;233:111517.
[6] Bargh HG, Sadr M. Stacking sequence optimization of composite plates for maximum fundamental frequency using particle swarm optimization algorithm. Meccanica 2012;47(3):719–30.
[7] Miller B, Ziemiański L. Optimization of dynamic behavior of thin-walled laminated cylindrical shells by genetic algorithms and deep neural networks supported by modal shape identification. Adv Eng Softw 2020;147:102830.
[8] Bharti K, Kumaraswamidhas LA, Das RR. A novel optimization approach for bonded tubular gap K-joints made of FRP composites. Structures 2020;28:2135–45.
[9] Apalak MK, Karaboga D, Akay B. The Artificial Bee Colony algorithm in layer optimization for the maximum fundamental frequency of symmetrical laminated composite plates. Eng Optim 2014;46(3):420–37.
[10] Ho-Huu V, Do-Thi TD, Dang-Trung H, Vo-Duy T, Nguyen-Thoi T. Optimization of laminated composite plates for maximizing buckling load using improved differential evolution and smoothed finite element method. Compos Struct 2016;146:132–47.
[11] Roque CMC, Marti PALS. Differential evolution for optimization of functionally graded beams. Compos Struct 2015;133:1191–7.
[12] Liu Q. Exact sensitivity analysis of stresses and lightweight design of Timoshenko composite beams. Compos Struct 2016;143:272–86.
[13] Vo-Duy T, Duong-Gia D, Ho-Huu V, Vu-Do HC, Nguyen-Thoi T. Multi-objective optimization of laminated composite beam structures using NSGA-II algorithm. Compos Struct 2017;168:498–509.
[14] Tanaka H, Mori Y, Kumekawa N, Matsuzaki R. Multi-objective optimization of weight and strength of laminated composites using gap-less and overlap-less variable thickness fiber placement. Compos Struct 2021;276:114562.

[15] Serhat G, Basdogan I. Multi-objective optimization of composite plates using lamination parameters. Mater Des 2019;180:107904.
[16] Abo-bakr RM, Shanab RA, Attia MA. Multi-objective optimization for lightweight design of bi-directional functionally graded beams for maximum frequency and buckling load. Compos Struct 2021;278:114691.
[17] Peng X, Guo Y, Li J, Wu H, Jiang S. Multiple objective optimization design of hybrid composite structures considering multiple-scale uncertainties. Compos Struct 2022;292:115658.
[18] Seyyedrahmani F, Khandar Shahabad P, Serhat G, Bediz B, Basdogan I. Multi-objective optimization of composite sandwich panels using lamination parameters and spectral Chebyshev method. Compos Struct 2022;289:115417.
[19] Radebe IS, Drosopoulos GA, Adali S. Buckling of non-uniformly distributed graphene and fibre reinforced multiscale angle-ply laminates. Meccanica 2019;54 (14):2263–79.
[20] Guo H, Cao S, Yang T, Chen Y. Vibration of laminated composite quadrilateral plates reinforced with graphene nanoplatelets using the element-free IMLS-Ritz method. Int J Mech Sci 2018;142–143:610–21.
[21] Lu SF, Li HJ, Zhang W, Song XJ. Vibration reduction of FG-CNTR piezoelectric laminated composite cantilever plate under aerodynamic load using full-dimensional state observer. Eng Struct 2022;255:113942.
[22] Jin Q. A new electro-mechanical finite formulation for functionally graded graphene reinforced composite laminated thick plates with piezoelectric actuator. Thin-Walled Struct 2022;176:109190.
[23] Rout M, Hota SS, Karmakar A. Thermoelastic free vibration response of graphene reinforced laminated composite shells. Eng Struct 2019;178:179–90.
[24] Kiani Y. Isogeometric large amplitude free vibration of graphene reinforced laminated plates in thermal environment using NURBS formulation. Computer Methods in Appled Mechanics and Engineering 2018;332:86–101.
[25] Saidi AR, Bahaadini R, Majidi-Mozafari K. On vibration and stability analysis of porous plates reinforced by graphene platelets under aerodynamical loading. Compos B Eng 2019;164:778–99.
[26] El-Ashmawy AM, Xu Y, El-Mahdy LA. Mechanical properties improvement of bi-directional functionally graded laminated MWCNT reinforced composite beams using an integrated tailoring–optimization approach. Microporous Mesoporous Mater 2021;314:110875.
[27] Dat ND, Quan TQ, Duc ND. Nonlinear thermal dynamic buckling and global optimization of smart sandwich plate with porous homogeneous core and carbon nanotube reinforced nanocomposite layers. Eur J Mech A Solids 2021;90:104351.
[28] Albak EI, Solmaz E, Yıldız AR, Öztürk F. Multiobjective crashworthiness optimization of graphene type multi-cell tubes under various loading conditions. J Braz Soc Mech Sci Eng 2021;43:266.
[29] Dat ND, Quan TQ, Tran P, Lam PT, Duc ND. A first-principle study of nonlinear large amplitude vibration and global optimization of 3D penta-graphene plates based on the Bees Algorithm. Acta Mech 2020;231(9):3799–823.
[30] Kamarian S, Shakeri M, Yas MH. Natural frequency analysis and optimal design of CNT/fiber/polymer hybrid composites plates using mori-tanaka approach, GDQ technique, and firefly algorithm. Polym Compos 2018;39(5):1433–46.
[31] Savran M, Aydin L. Stochastic optimization of graphite-flax/epoxy hybrid laminated composite for maximum fundamental frequency and minimum cost. Eng Struct 2018;174:675–87.
[32] Hosseinzadeh Y, Jalili S, Khani R. Investigating the effects of flax fibers application on multi-objective optimization of laminated composite plates for simultaneous cost minimization and frequency gap maximization. Journal of Building Engineering 2020;32:101477.
[33] Jalili S, Khani R, Hosseinzadeh Y. On the performance of flax fibres in multi-objective design of laminated composite plates for buckling and cost. Structures 2021;33:3094–106.
[34] An H, Chen S, Huang H. Multi-objective optimal design of hybrid composite laminates for minimum cost and maximum fundamental frequency and frequency gaps. Compos Struct 2019;209:268–76.
[35] Jeawon Y, Drosopoulos GA, Foutsitzi G, Stavroulakis GE, Adali S. Optimization and analysis of frequencies of multi-scale graphene/fibre reinforced nanocomposite laminates with non-uniform distributions of reinforcements. Eng Struct 2021;228: 111525.
[36] Reddy JN. Mechanics of laminated composite plates and shells: theory and analysis. 2nd ed. Boca Raton: CRC Press; 2004.
[37] Huang Y, Yang Z, Liu A, Fu J. Nonlinear buckling analysis of functionally graded graphene reinforced composite shallow arches with elastic rotational constraints under uniform radial load. Materials 2018;11(6):910.
[38] Yang J, Chen D, Kitipornchai S. Buckling and free vibration analyses of functionally graded graphene reinforced porous nanocomposite plates based on Chebyshev-Ritz method. Compos Struct 2018;193:281–94.
[39] Yang J, Wu H, Kitipornchai S. Buckling and postbuckling of functionally graded multilayer graphene platelet-reinforced composite beams. Compos Struct 2017; 161:111–8.
[40] Deb K, Pratap A, Agarwal S, Meyarivan T. A fast and elitist multiobjective genetic algorithm: NSGA-II. IEEE Trans Evol Comput 2002;6:182–97.
[41] Deb K, Jain H. An Evolutionary Many-Objective Optimization Algorithm Using Reference-Point-Based Nondominated Sorting Approach, Part I: Solving Problems With Box Constraints. IEEE Trans Evol Comput 2014;18(4):577–601.
[42] Tian Ye, Cheng R, Zhang X, Jin Y. PlatEMO: A MATLAB Platform for Evolutionary Multi-Objective Optimization [Educational Forum]. IEEE Comput Intell Mag 2017; 12(4):73–87.
[43] Civalek O, Dastjerdi S, Akgöz B. Buckling and free vibrations of CNT-reinforced cross-ply laminated composite plates. Mech Based Des Struct Mach 2020;50(6): 1914–31.
[44] Lei ZX, Zhang LW, Liew KM. Free vibration analysis of laminated FG-CNT reinforced composite rectangular plates using the kp-Ritz method. Compos Struct 2015;127:245–59.